

## Next-to-leading order QCD corrections to the production of $B_c$ and $B_c^*$ through $W^+$ -boson decays

Xu-Chang Zheng,<sup>1,\*</sup> Chao-Hsi Chang,<sup>2,3,4,†</sup> Xing-Gang Wu<sup>⊗</sup>,<sup>1,‡</sup> Jun Zeng,<sup>1,§</sup> and Xu-Dong Huang<sup>1,||</sup>

<sup>1</sup>*Department of Physics, Chongqing University, Chongqing 401331, People's Republic of China*

<sup>2</sup>*Key Laboratory of Theoretical Physics, Institute of Theoretical Physics, Chinese Academy of Sciences, Beijing 100190, China*

<sup>3</sup>*School of Physical Sciences, University of Chinese Academy of Sciences, Beijing 100049, China*

<sup>4</sup>*CCAST (World Laboratory), Beijing 100190, China*



(Received 1 December 2019; accepted 3 February 2020; published 24 February 2020)

In this paper, we calculate the total decay widths for the  $W^+$ -boson decays,  $W^+ \rightarrow B_c + b + \bar{s} + X$  and  $W^+ \rightarrow B_c^* + b + \bar{s} + X$ , up to next-to-leading order (NLO) accuracy within the framework of the nonrelativistic QCD theory. Both the fixed-order and the fragmentation approaches are adopted to do the calculation. Differential decay widths  $d\Gamma/dz$  and  $d\Gamma/ds_1$  are also given. We find that the NLO corrections are significant in those two  $W^+$  decay channels. Our numerical results show that at the LHC, there are about  $7.03 \times 10^4$   $B_c$ -meson events and  $5.10 \times 10^4$   $B_c^*$ -meson events to be produced via the  $W^+$ -boson decays per operation year.

DOI: [10.1103/PhysRevD.101.034029](https://doi.org/10.1103/PhysRevD.101.034029)

### I. INTRODUCTION

The  $(c\bar{b})$ -quarkonium is a unique system in the Standard Model (SM) which carries two different heavy flavors. Studies on its production, decay, and mass spectrum, etc., provide us a good platform to understand the strong and weak interactions deeply. The ground state  $B_c$  meson was first observed by the CDF collaboration at the Tevatron [1] and it has attracted lots of interest since then. At present, the direct production of the  $B_c$  meson and its excited states have been studied extensively in  $pp$  [2–18],  $e^+e^-$  [19–24] and  $ep$  [25,26] collisions.

Besides the direct production mechanisms, the  $B_c$  meson can also be indirectly produced through the top-quark [27–29], the  $Z^0$ -boson [30–34], the Higgs-boson [35,36] and the  $W$ -boson [37–39] decays. These indirect production channels can also generate abundant  $B_c$  mesons at the LHC or the future high-energy colliders. The  $W$ -boson is the propagating media for the weak interaction, and the study on it is important for testing the SM. The LHC is a fruitful  $W$ -boson factory; there are about  $3.07 \times 10^{10}$

$W$ -bosons to be produced at the LHC per operation year [37]. In the paper, we shall concentrate on the production of the  $B_c$  meson and its first excited state  $B_c^*$  meson through the  $W$ -boson decays.

The heavy constituent quarks move nonrelativistically in the  $B_c$  meson, and the processes involving the  $B_c$  meson can be calculated within the nonrelativistic QCD (NRQCD) factorization formalism [40]. Generally, the production cross section or the decay width can be factorized into the product of the short-distance coefficients and the long-distance matrix elements. The short-distance coefficients describe the production or decay rate of the heavy quark-antiquark pair, which can be perturbatively calculated in powers of the strong coupling constant  $\alpha_s(m_Q)$ . The nonperturbative long-distance matrix elements describe the formation of the  $B_c$  meson from the heavy quark-antiquark pair, which can be calculated through potential models or lattice QCD.

The excited states of the  $B_c$  meson shall directly or indirectly decay to the ground state  $B_c$  meson via electromagnetic or strong interactions with  $\sim 100\%$  probability, so these excited states are important sources of the  $B_c$  meson. Moreover, the production of the excited state is also interesting by itself. So, in addition to the  $B_c$ -meson production, we shall also consider the production of the spin-triplet  $^3S_1$  state  $B_c^*$ . The production of  $B_c$  and  $B_c^*$  mesons via the  $W$ -boson decays at the leading order (LO) level has been studied in Refs. [37,38]. Since the masses of  $b$  and  $c$  quarks are not too large compared to the QCD asymptotic scale  $\Lambda_{\text{QCD}}$ , the higher-order QCD corrections could be important. In this paper, we shall study the

\*zhengxc@cqu.edu.cn

†zhangzx@itp.ac.cn

‡wuxg@cqu.edu.cn

§zengj@cqu.edu.cn

||hxud@cqu.edu.cn

Published by the American Physical Society under the terms of the [Creative Commons Attribution 4.0 International license](https://creativecommons.org/licenses/by/4.0/). Further distribution of this work must maintain attribution to the author(s) and the published article's title, journal citation, and DOI. Funded by SCOAP<sup>3</sup>.

$B_c^{(*)}$ -meson production via the  $W$ -boson decays up to next-to-leading order (NLO) accuracy.

There are two decay channels for the inclusive  $B_c$  production through the  $W^+$ -boson decays at  $\mathcal{O}(\alpha_s^2)$ , i.e.,  $W^+ \rightarrow B_c + b + \bar{s}$  and  $W^+ \rightarrow B_c + c + \bar{c}$ . Due to the double suppression from the small value of  $|V_{cb}|$  and the smaller phase space, the contribution from the decay channel  $W^+ \rightarrow B_c + c + \bar{c}$  is greatly depressed. More explicitly, we have [38]  $\Gamma_{W^+ \rightarrow B_c + c + \bar{c}}/\Gamma_{W^+ \rightarrow B_c + c + \bar{s}} = 0.086$  and  $\Gamma_{W^+ \rightarrow B_c^* + c + \bar{c}}/\Gamma_{W^+ \rightarrow B_c^* + c + \bar{s}} = 0.150$  at the LO level. Thus, in this paper, we only consider the decay channels  $W^+ \rightarrow B_c^{(*)} + b + \bar{s} + X$ .

Any physical observable is independent of the renormalization scale, but there is renormalization scale ambiguity for the fixed-order pQCD predictions since one usually guesses the renormalization scale (e.g., usually setting as the one to eliminate large logs etc.) and varies it over an arbitrary range to ascertain its uncertainty. This ambiguity introduces an important systematic error to pQCD predictions. It has been pointed out that one can use the higher-order  $\beta$ -terms to achieve an effective value of the strong running coupling  $\alpha_s$ , and the resultant conformal series is independent to the choice of renormalization scale and thus the conventional renormalization ambiguity is eliminated [41–43]. The principle of maximum conformality (PMC) has been designed for such a purpose [44–48], which provides a systemic way to eliminate the renormalization scheme-and-scale ambiguities simultaneously. The key idea of PMC is to set the correct momentum flow of the process by absorbing the nonconformal  $\beta$ -terms that govern the behavior of  $\alpha_s$  through the renormalization group equation (RGE). The  $\beta_0$ -terms in the NLO coefficients can be adopted to set the  $\alpha_s$  value, thus in the paper, in addition to the conventional treatment, we shall also adopt the PMC to deal with the  $W^+$ -boson decays,  $W^+ \rightarrow B_c^{(*)} + b + \bar{s} + X$ .

In the decays,  $W^+ \rightarrow B_c^{(*)} + b + \bar{s} + X$ , the involved hard scales satisfy,  $m_W \gg m_b, m_c$ , so it is expected that the fragmentation mechanism dominates those decays. The NLO fragmentation functions for a heavy quark to a  $B_c$  or  $B_c^*$  have recently been given by Ref. [23]. It is interesting to apply those NLO fragmentation functions to the present processes, and compare the results from the fragmentation approach with those from the fixed-order approach. In the present paper, besides the fixed-order approach, we shall also adopt the fragmentation approach to do the calculation. In usual cases, because the fragmentation probability of  $\bar{b} \rightarrow B_c$  is about 2 orders of magnitude larger than that of  $c \rightarrow B_c$ , the  $\bar{b}$  fragmentation is generally more important than the  $c$  fragmentation for the  $B_c$ -meson production. However, in cases with the  $W^+$ -boson decays, the decay width for the  $\bar{b}$  fragmentation shall be depressed due to the small values of the Cabibbo-Kobayashi-Maskawa (CKM) matrix elements  $|V_{cb}|$  and  $|V_{ub}|$ ; thus, it provides a good platform to test the fragmentation function for  $c \rightarrow B_c$ .

The paper is organized as follows. In Sec. II, we briefly present useful formulas at the LO accuracy under the fixed-order approach. In Sec. III, we present the formulas to calculate the NLO QCD corrections for the  $B_c^{(*)}$ -meson production through the  $W$ -boson decays under the fixed-order approach. In Sec. IV, we present the useful formulas to calculate the decay widths under the fragmentation approach up to NLO accuracy. In Sec. V, numerical results and discussions are presented. Section VI is reserved as a summary.

## II. DECAY WIDTHS AT THE LO LEVEL

According to the NRQCD factorization, the differential decay width for the  $B_c$ -meson production from the  $W^+$ -boson decays can be written as

$$d\Gamma_{W^+ \rightarrow B_c + b + \bar{s} + X} = \sum_n d\tilde{\Gamma}_{W^+ \rightarrow (c\bar{b})[n] + b + \bar{s} + X} \langle \mathcal{O}^{B_c}(n) \rangle, \quad (1)$$

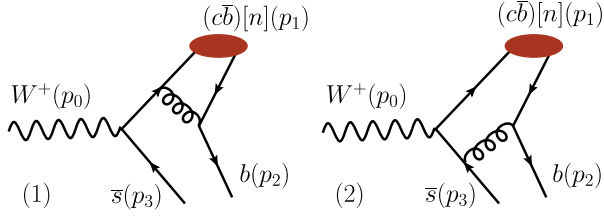
where  $d\tilde{\Gamma}_{W^+ \rightarrow (c\bar{b})[n] + b + \bar{s} + X}$  denotes the decay width for the production of a perturbative state  $(c\bar{b})[n]$  with quantum numbers  $[n]$ . The long-distance matrix element  $\langle \mathcal{O}^{B_c}(n) \rangle$  is the transition probability for a  $(c\bar{b})[n]$  state to the  $B_c$  meson. In the lowest-order nonrelativistic approximation, only color-singlet contributions need to be considered, and the long-distance matrix elements for the color-singlet contributions can be determined through potential models.

Practically, we first calculate the decay width for an on-shell  $(c\bar{b})$ -pair, i.e.,  $d\Gamma_{W^+ \rightarrow (c\bar{b})[n] + b + \bar{s} + X}$ . Then the decay width for the  $B_c$  meson, i.e.,  $d\Gamma_{W^+ \rightarrow B_c + b + \bar{s} + X}$ , can be obtained from  $d\Gamma_{W^+ \rightarrow (c\bar{b})[n] + b + \bar{s} + X}$  by replacing  $\langle \mathcal{O}^{(c\bar{b})[n]}(n) \rangle$  by  $\langle \mathcal{O}^{B_c}(n) \rangle$ .

At the LO level, there are two Feynman diagrams for the  $(c\bar{b})[n]$ -pair production from the  $W^+$ -boson decays, which are shown in Fig. 1. The LO amplitude for the  $(c\bar{b})[n]$  production can be written as the sum of two terms ( $M_{\text{LO}} = M_1 + M_2$ ) corresponding to two Feynman diagrams in Fig. 1, and we have

$$iM_1 = -\frac{igV_{cs}}{2\sqrt{2}} \frac{-i}{(p_{12} + p_2)^2 + i\epsilon} \bar{u}(p_2)(ig_s\gamma^\mu T^a) \cdot \Pi\Lambda_1(ig_s\gamma_\mu T^a) \frac{i}{\not{p}_1 + \not{p}_2 - m_c + i\epsilon} \cdot e_\nu(p_0)\gamma^\nu(1 - \gamma_5)v(p_3)|_{q=0}, \quad (2)$$

$$iM_2 = -\frac{igV_{cs}}{2\sqrt{2}} \frac{-i}{(p_{12} + p_2)^2 + i\epsilon} \bar{u}(p_2)(ig_s\gamma^\mu T^a)\Pi\Lambda_1 \cdot e_\nu(p_0)\gamma^\nu(1 - \gamma_5) \frac{i}{-\not{p}_0 + \not{p}_{11} + i\epsilon} \cdot (ig_s\gamma_\mu T^a)v(p_3)|_{q=0}, \quad (3)$$


 FIG. 1. The LO Feynman diagrams for  $W^+ \rightarrow (c\bar{b})[n] + b + \bar{s}$ .

where  $p_{11}$  and  $p_{12}$  are momenta of the  $c$  and  $\bar{b}$  quarks in the  $(c\bar{b})[n]$ -pair,

$$p_{11} = r_c p_1 - q, \quad p_{12} = (1 - r_c) p_1 + q, \quad (4)$$

where  $r_c = m_c/(m_b + m_c)$ .  $\Pi$  denotes the spin projector, for the  $^1S_0$  state,

$$\Pi = \frac{-\sqrt{M}}{4m_b m_c} (\not{p}_{12} - m_b) \gamma_5 (\not{p}_{11} + m_c), \quad (5)$$

and for the  $^3S_1$  state,

$$\Pi = \frac{-\sqrt{M}}{4m_b m_c} (\not{p}_{12} - m_b) \not{p}_1 (\not{p}_{11} + m_c). \quad (6)$$

$\Lambda_1$  is the color-singlet projector, and

$$\Lambda_1 = \frac{\mathbf{1}}{\sqrt{3}}, \quad (7)$$

where  $\mathbf{1}$  denotes the unit matrix of the color  $SU(3)$  group.

Using those amplitudes at the LO level, the LO decay width for  $(c\bar{b})$ -pair production can be calculated through

$$d\Gamma_{\text{LO}}^{(c\bar{b})[n]} = \frac{1}{3} \frac{1}{2m_W} \sum |M_{\text{LO}}|^2 d\Phi_3, \quad (8)$$

where  $\sum$  denotes the sum over the color and spin states of the initial and final particles,  $1/3$  comes from the spin average of the initial  $W^+$ -boson.  $d\Phi_3$  denotes the differential phase space at the LO level,

$$d\Phi_3 = (2\pi)^d \delta^d \left( p_0 - \sum_{f=1}^3 p_f \right) \prod_{f=1}^3 \frac{d^{d-1} \mathbf{p}_f}{(2\pi)^{d-1} 2E_f}, \quad (9)$$

where  $d$  stands for the dimension of the space-time. With these formulas, the LO decay width for  $W^+ \rightarrow (c\bar{b})[n] + b + \bar{s} + X$  can be calculated directly.

### III. THE NLO QCD CORRECTIONS

The NLO QCD corrections to the decay widths include virtual and real corrections. There are ultraviolet (UV) and infrared (IR) divergences in virtual correction, and IR

divergence in real correction. We adopt the conventional dimensional regularization approach with  $d = 4 - 2\epsilon$  to regulate these divergences. Then the UV and IR divergences appear as pole terms in  $1/\epsilon$ . We shall sketch the calculations for the virtual and real corrections in the following subsections.

#### A. The virtual correction

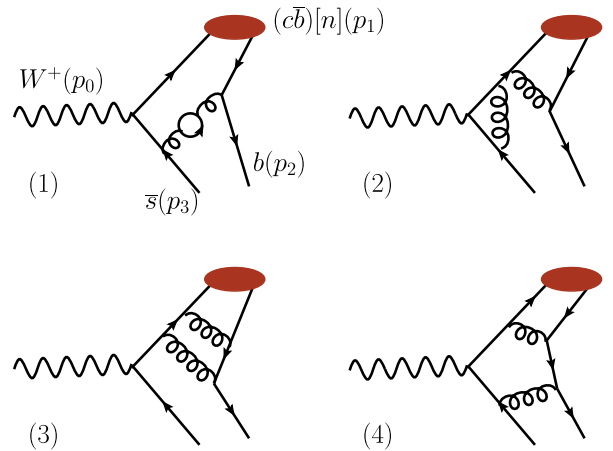
Four typical one-loop diagrams are shown in Fig. 2. The NLO virtual corrections come from the interference of those one-loop Feynman diagrams with the LO Feynman diagrams shown in Fig. 1.

The virtual corrections can be calculated through

$$d\Gamma_{\text{Virtual}}^{(c\bar{b})[n]} = \frac{1}{3} \frac{1}{2m_W} \sum 2\text{Re}(M_{\text{LO}}^* M_{\text{Virtual}}) d\Phi_3, \quad (10)$$

where  $M_{\text{Virtual}}$  denotes the amplitude for the virtual corrections,  $d\Phi_3$  is the LO differential phase space.

As a subtle point, there are Coulomb divergences in the hard part of the NLO amplitudes by using the traditional matching procedure. One may observe that they appear in both the virtual corrections to the  $(c\bar{b})[n]$  production and the virtual corrections to the long-distance matrix element  $\langle \mathcal{O}^{(c\bar{b})[n]}(n) \rangle$ , which shall be canceled by each other. As a result, no Coulomb divergence appears in the resultant pQCD series. In dimensional regularization, there is a simpler way to extract the NRQCD short-distance coefficients using the method of regions [49]. In this method, one can calculate the hard region contributions directly by expanding the relative momentum of the  $(c\bar{b})[n]$  pair before carrying out the loop integration (more explicitly, under the present lowest-order nonrelativistic approximation, one just needs to set  $q = 0$  before the loop integration). Then the Coulomb divergences, which are power IR divergences, vanish in dimensional regularization. We adopt this new


 FIG. 2. Four typical one-loop Feynman diagrams for  $W^+ \rightarrow c\bar{b}[n] + b + \bar{s}$ .

treatment, and the Coulomb divergences shall not appear in our present calculation.

There are UV and IR divergences in the loop-diagram contributions. The IR divergences in the virtual correction shall be canceled by the IR divergences in the real correction. The UV divergences should be removed through renormalization. We carry out the renormalization using the counterterm approach, where the decay widths are calculated in terms of the renormalized quark mass  $m$ , the renormalized quark field  $\Psi_r$ , the renormalized gluon field  $A_r^\mu$ , and the renormalized coupling constant  $g_s$ . The relations between the renormalized quantities and their corresponding bare quantities are

$$\begin{aligned} m_0 &= Z_m m, & \Psi_0 &= \sqrt{Z_2} \Psi_r, \\ A_0^\mu &= \sqrt{Z_3} A_r^\mu, & g_s^0 &= Z_g g_s, \end{aligned} \quad (11)$$

where  $Z_i = 1 + \delta Z_i$  with  $i = m, 2, 3, g$  are renormalization constants, and they are fixed by the renormalization scheme. The renormalization scheme is adopted as follows: The renormalization of the heavy quark mass, the heavy quark field, the light quark field and the gluon field are performed in the on-shell scheme, whereas the renormalization of the strong coupling constant is performed in the  $\overline{\text{MS}}$  scheme. The quantities  $\delta Z_i$  can be calculated and they are

$$\begin{aligned} \delta Z_{m,Q}^{\text{OS}} &= -3C_F \frac{\alpha_s}{4\pi} \left[ \frac{1}{\epsilon_{\text{UV}}} - \gamma_E + \ln \frac{4\pi\mu_R^2}{m_Q^2} + \frac{4}{3} \right], \\ \delta Z_{2,Q}^{\text{OS}} &= -C_F \frac{\alpha_s}{4\pi} \left[ \frac{1}{\epsilon_{\text{UV}}} + \frac{2}{\epsilon_{\text{IR}}} - 3\gamma_E + 3 \ln \frac{4\pi\mu_R^2}{m_Q^2} + 4 \right], \\ \delta Z_{2,q}^{\text{OS}} &= -C_F \frac{\alpha_s}{4\pi} \left[ \frac{1}{\epsilon_{\text{UV}}} - \frac{1}{\epsilon_{\text{IR}}} \right], \\ \delta Z_3^{\text{OS}} &= \frac{\alpha_s}{4\pi} \left[ (\beta'_0 - 2C_A) \left( \frac{1}{\epsilon_{\text{UV}}} - \frac{1}{\epsilon_{\text{IR}}} \right) \right. \\ &\quad \left. - \frac{4}{3} T_F \left( \frac{1}{\epsilon_{\text{UV}}} - \gamma_E + \ln \frac{4\pi\mu_R^2}{m_c^2} \right) \right. \\ &\quad \left. - \frac{4}{3} T_F \left( \frac{1}{\epsilon_{\text{UV}}} - \gamma_E + \ln \frac{4\pi\mu_R^2}{m_b^2} \right) \right], \\ \delta Z_g^{\overline{\text{MS}}} &= -\frac{\beta'_0}{2} \frac{\alpha_s}{4\pi} \left[ \frac{1}{\epsilon_{\text{UV}}} - \gamma_E + \ln(4\pi) \right], \end{aligned}$$

where  $Q(=c, b)$  in the subscripts denotes a heavy quark, and  $q(=s)$  denotes a light quark.  $\mu_R$  is the renormalization scale,  $\gamma_E$  is the Euler constant. For QCD,  $C_A = 3$ ,  $C_F = 4/3$  and  $T_F = 1/2$ .  $\beta'_0 = 11C_A/3 - 4T_F n_f/3$  is the one-loop coefficient of the QCD  $\beta$  function, in which  $n_f$  is the number of active quark flavors.  $\beta'_0 = 11C_A/3 - 4T_F n_{lf}/3$  and  $n_{lf} = 3$  is the number light-quark flavors.

## B. The real correction

The real corrections come from the decay process  $W^+(p_0) \rightarrow (c\bar{b})[n](p_1) + b(p_2) + \bar{s}(p_3) + g(p_4)$ . The Feynman diagrams for the real corrections can be obtained through the LO Feynman diagrams by adding an additional gluon in the final state. Typical real correction Feynman diagrams are shown in Fig. 3. The real correction can be calculated through

$$d\Gamma_{\text{Real}}^{(c\bar{b})[n]} = \frac{1}{3} \frac{1}{2m_W} \sum |M_{\text{Real}}|^2 d\Phi_4, \quad (12)$$

where  $d\Phi_4$  denotes the differential phase space for the real corrections, and

$$d\Phi_4 = (2\pi)^d \delta^d \left( p_0 - \sum_{f=1}^4 p_f \right) \prod_{f=1}^4 \frac{d^{d-1} \mathbf{p}_f}{(2\pi)^{d-1} 2E_f}. \quad (13)$$

There are IR divergences in the real correction, which come from the phase-space integration. However, integrating the squared amplitude directly over the phase space in  $d$  dimensions is too difficult to be practical. In order to isolate the divergent and finite terms, we adopt the two-cutoff phase-space slicing method [50] to calculate the real correction. Following this method, the phase space for the real correction is decomposed into three regions by introducing two small cutoffs,  $\delta_s$  and  $\delta_c$ , which should satisfy the requirement  $\delta_c \ll \delta_s$  [50]. The three regions are the soft region (S) with  $E_4 \leq m_W \delta_s/2$ , hard-collinear region (HC) with  $E_4 > m_W \delta_s/2$  and  $(p_3 + p_4)^2 \leq \delta_c m_W^2$ , and hard-noncollinear region (HC $\bar{C}$ ) with  $E_4 > m_W \delta_s/2$  and  $(p_3 + p_4)^2 > \delta_c m_W^2$ , where  $E_4$  is defined in the rest frame of the initial  $W^+$ -boson. The IR finite hard-noncollinear part can be calculated numerically in four dimensions.

Applying the soft approximation to the soft part (e.g., all the terms of order  $\delta_s$  are neglected), we obtain

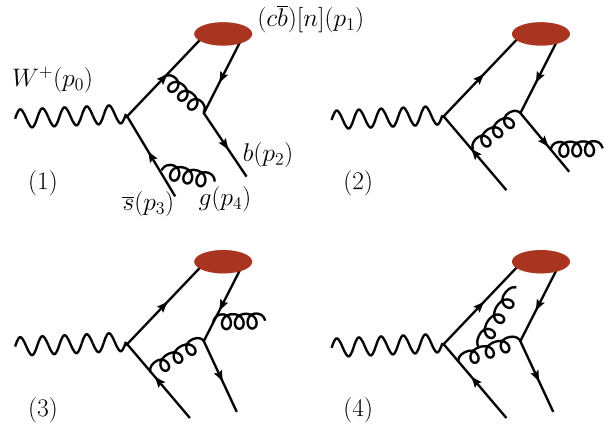


FIG. 3. Four typical real-correction Feynman diagrams for  $W^+ \rightarrow (c\bar{b})[n] + b + \bar{s}$ .

$$\begin{aligned}
d\Gamma_S^{(c\bar{b})[n]} &= d\Gamma_{\text{LO}}^{(c\bar{b})[n]} \left[ \frac{C_F \alpha_s}{2\pi} \frac{\Gamma(1-\epsilon)}{\Gamma(1-2\epsilon)} \left( \frac{4\pi\mu_R^2}{m_W^2} \right)^\epsilon \right] \\
&\cdot \left\{ \frac{1}{\epsilon^2} + \frac{1}{\epsilon} \left[ 1 - 2 \ln \delta_s - \ln \left( \frac{(1-\beta_b \cos \theta)^2}{1-\beta_b^2} \right) \right] - 2 \ln \delta_s + 2 \ln^2 \delta_s + 2 \ln \delta_s \ln \left( \frac{(1-\beta_b \cos \theta)^2}{1-\beta_b^2} \right) \right. \\
&+ \frac{1}{\beta_b} \ln \left( \frac{1+\beta_b}{1-\beta_b} \right) + \ln^2 \left( \frac{1-\beta_b}{1-\beta_b \cos \theta} \right) - \frac{1}{2} \ln^2 \left( \frac{1+\beta_b}{1-\beta_b} \right) + 2 \text{Li}_2 \left( -\frac{\beta_b(1-\cos \theta)}{1-\beta_b} \right) \\
&\left. - 2 \text{Li}_2 \left( -\frac{\beta_b(1+\cos \theta)}{1-\beta_b \cos \theta} \right) \right\}, \tag{14}
\end{aligned}$$

where  $\beta_b = \sqrt{1 - m_b^2/E_2^2}$ , and  $E_2$  is defined in the rest frame of the  $W^+$ -boson.  $\theta$  is the angle between  $\mathbf{p}_2$  and  $\mathbf{p}_3$  in the rest frame of the  $W^+$ -boson.

Applying the collinear approximation (e.g., terms of order  $\delta_c$  are neglected), we obtain

$$\begin{aligned}
d\Gamma_{\text{HC}}^{(c\bar{b})[n]} &= d\Gamma_{\text{LO}}^{(c\bar{b})[n]} \left[ \frac{C_F \alpha_s}{2\pi} \frac{\Gamma(1-\epsilon)}{\Gamma(1-2\epsilon)} \left( \frac{4\pi\mu_R^2}{m_W^2} \right)^\epsilon \right] \\
&\times \left( \frac{A_1^{q \rightarrow qg}}{\epsilon} + A_0^{q \rightarrow qg} \right), \tag{15}
\end{aligned}$$

where

$$A_1^{q \rightarrow qg} = 3/2 + 2 \ln \delta'_s, \tag{16}$$

$$A_0^{q \rightarrow qg} = 7/2 - \pi^2/3 - \ln^2 \delta'_s - \ln \delta_c (3/2 + 2 \ln \delta'_s), \tag{17}$$

and  $\delta'_s = m_W^2 \delta_s / [m_W^2 - (p_1 + p_2)^2]$ .

Summing up three parts from the soft, hard-collinear and hard-noncollinear regions, we obtain the required real correction. Separate contributions from three regions depend on one or both of the two cutoff parameters  $\delta_s$  and  $\delta_c$ . However, the sum of those three contributions should be independent to the choices of  $\delta_s$  and  $\delta_c$ . The verification of this cutoff independence provides an important check for the correctness of the numerical calculation. We have checked this independence and have indeed found that the results are independent of the  $\delta_s$  and  $\delta_c$  by varying  $\delta_s$  from  $10^{-3}$  to  $10^{-7}$  with  $\delta_c = \delta_s/50$ . For clarity, we fix  $\delta_s = 10^{-5}$  and  $\delta_c = 2 \times 10^{-7}$  to do the following numerical calculation.

Total NLO corrections can be obtained by summing up virtual and real corrections. The UV and IR divergences are exactly canceled after summing the real and virtual corrections, and the finite NLO corrections are obtained. Then the decay widths  $\Gamma_{W^+ \rightarrow B_c + b + \bar{s} + X}$  and  $\Gamma_{W^+ \rightarrow B_c^* + b + \bar{s} + X}$  can be derived from  $\Gamma_{W^+ \rightarrow (c\bar{b})[^1S_0] + b + \bar{s} + X}$  and  $\Gamma_{W^+ \rightarrow (c\bar{b})[^3S_1] + b + \bar{s} + X}$  by multiplying a factor  $\langle \mathcal{O}^{B_c(B_c^*)}(n) \rangle / \langle \mathcal{O}^{(c\bar{b})[n]}(n) \rangle \approx |R_S(0)|^2 / 4\pi$ , where  $n = ^1S_0$  for  $B_c$  and  $n = ^3S_1$  for  $B_c^*$ , respectively.  $R_S(0)$  denotes the radial wave function at the origin of the  $B_c(B_c^*)$  meson.

In the calculation, we adopt the FeynArts package [51] to generate the Feynman diagrams and the corresponding amplitudes, and the FeynCalc package [52,53] to carry out the Dirac and color traces. Then we use the \$Apart package [54] and the FIRE package [55] to do partial fraction and integration-by-parts (IBP) reduction of the loop integrals. After the IBP reduction, only a few master integrals (e.g.,  $A_0$ ,  $B_0$ ,  $C_0$ , and  $D_0$  functions) need to be calculated, which shall be dealt with by using the LoopTools package [56]. Numerical phase-space integrations are carried out by the VEGAS program [57].

#### IV. DECAY WIDTHS UNDER THE FRAGMENTATION APPROACH

We take the process  $W^+ \rightarrow B_c + X$  as an example to illustrate the calculation under the fragmentation approach. The formulas for the  $B_c^*$  production are similar to the  $B_c$  case.

The differential decay width for  $W^+ \rightarrow B_c + X$  under the fragmentation approach can be written as

$$\begin{aligned}
\frac{d\Gamma_{W^+ \rightarrow B_c + X}}{dz} &= \sum_i \int_z^1 \frac{dy}{y} \frac{d\hat{\Gamma}_{W^+ \rightarrow i + X}(y, \mu_F)}{dy} \\
&\cdot D_{i \rightarrow B_c}(z/y, \mu_F), \tag{18}
\end{aligned}$$

where  $d\hat{\Gamma}_{W^+ \rightarrow i + X}(y, \mu_F)$  denotes the decay width (coefficient function) for a  $W^+$  to a parton  $i$ ,<sup>1</sup>  $D_{i \rightarrow B_c}(z/y, \mu_F)$  denotes the fragmentation function for a parton  $i$  into a  $B_c$ , and  $\mu_F$  is the factorization scale which separates the energy scales of two parts.

For comparison, we adopt several strategies to obtain the fragmentation predictions. More details about those strategies can be found in Refs. [23,58]. For convenience, we

<sup>1</sup>Due to the coefficient function  $d\hat{\Gamma}_{W^+ \rightarrow i + X}(y, \mu_F)$  is IR safe, the heavy-quark mass  $m_Q$  in the coefficient function can be approximately set to 0, and this approximation brings only a small error of  $\mathcal{O}(m_Q^2/m_W^2)$ . In the following fragmentation calculations, we shall adopt this approximation for simplicity. The neglected higher-power terms will be included in the results by combining the fixed-order and fragmentation approaches.

denote them as ‘‘Frag, LO,’’ ‘‘Frag, NLO’’ and ‘‘Frag, NLO + NLL,’’ respectively. For the case of Frag, LO,

$$\begin{aligned} \frac{d\Gamma_{W^+ \rightarrow B_c + X}^{\text{Frag, LO}}}{dz} &= \int_z^1 \frac{dy}{y} \frac{d\hat{\Gamma}_{W^+ \rightarrow c + \bar{s}}^{\text{LO}}(y, \mu_F)}{dy} \cdot D_{c \rightarrow B_c}^{\text{LO}}(z/y, \mu_F) \\ &= \Gamma_{W^+ \rightarrow c + \bar{s}}^{\text{LO}} \cdot D_{c \rightarrow B_c}^{\text{LO}}(z, \mu_F), \end{aligned} \quad (19)$$

where  $\Gamma_{W^+ \rightarrow c + \bar{s}}^{\text{LO}}$  is the LO decay width for  $W^+ \rightarrow c + \bar{s}$  and  $D_{c \rightarrow B_c}^{\text{LO}}(z, \mu_F)$  is the LO fragmentation function. In the calculation, the factorization and renormalization scales are set as  $\mu_F = 2m_b + m_c$  and  $\mu_R = 2m_b$ .

For the case of Frag, NLO,

$$\begin{aligned} \frac{d\Gamma_{W^+ \rightarrow B_c + X}^{\text{Frag, NLO}}}{dz} &= \int_z^1 \frac{dy}{y} \frac{d\hat{\Gamma}_{W^+ \rightarrow c + X}^{\text{NLO}}(y, \mu_F)}{dy} \\ &\cdot D_{c \rightarrow B_c}^{\text{NLO}}(z/y, \mu_F), \end{aligned} \quad (20)$$

where the NLO fragmentation function  $D_{c \rightarrow B_c}^{\text{NLO}}(z, \mu_F)$  can be found in Ref. [23]. In the calculation, the factorization and renormalization scales are set as  $\mu_F = 2m_b + m_c$  and  $\mu_R = 2m_b$ , and the factorization scheme is chosen as the  $\overline{\text{MS}}$  scheme.

For the case of Frag, NLO + NLL,

$$\begin{aligned} \frac{d\Gamma_{W^+ \rightarrow B_c + X}^{\text{Frag, NLO+NLL}}}{dz} &= \int_z^1 \frac{dy}{y} \frac{d\hat{\Gamma}_{W^+ \rightarrow c + X}^{\text{NLO}}(y, \mu_F)}{dy} \\ &\cdot D_{c \rightarrow B_c}^{\text{NLO+NLL}}(z/y, \mu_F), \end{aligned} \quad (21)$$

where the upper factorization and renormalization scales in the coefficient function  $d\hat{\Gamma}_{W^+ \rightarrow c + X}^{\text{NLO}}(y, \mu_F)/dy$  are set as  $\mu_F = \mu_R = m_W$ , so as to avoid the large logarithms of  $\mu_F^2/m_W^2$  or  $\mu_R^2/m_W^2$  appear in the coefficient function. The fragmentation function  $D_{c \rightarrow B_c}^{\text{NLO+NLL}}(z, \mu_F = m_W)$  is obtained through solving the Dokshitzer-Gribov-Lipatov-Altarelli-Parisi (DGLAP) evolution equation [59–61] with NLO splitting function for  $c \rightarrow c$  [62–64], where the NLO fragmentation function  $D_{c \rightarrow B_c}^{\text{NLO}}(z, \mu_{F0} = 2m_b + m_c)$  with the lower factorization and renormalization scales  $\mu_{F0} = 2m_b + m_c$  and  $\mu_{R0} = 2m_b$  is used as the boundary condition. To solve the DGLAP evolution equation, the Mellin transformation method is adopted, and the related formulas for the Mellin transformation method can be found in Ref. [65].<sup>2</sup>

<sup>2</sup>In Ref. [65], the authors adopted an approximation that the singularity of the NLO splitting function  $P_{Q \rightarrow Q}(z)$  at  $z = 1$  is regularized by an overall ‘‘+’’ prescription. Then,  $\int_0^1 P_{c \rightarrow c}(z) dz = 0$ . This approximation is reasonable and applicable, since the probability to produce an additional heavy quark pair in the evolution process is very low at the energy of  $m_W$ . For simplicity, we shall adopt this approximation in the present paper.

## V. NUMERICAL RESULTS AND DISCUSSIONS

To do the numerical calculation, the input parameters are taken as follows:

$$\begin{aligned} m_b &= 4.9 \text{ GeV}, \quad m_c = 1.5 \text{ GeV}, \quad m_W = 80.4 \text{ GeV}, \\ G_F &= 1.166 \times 10^{-5} \text{ GeV}^{-2}, \quad |V_{cs}| = 1, \\ |R_S(0)|^2 &= 1.642 \text{ GeV}^3, \end{aligned} \quad (22)$$

where  $G_F$  is the Fermi coupling constant. The input value for  $|R_S(0)|^2$  is taken from the potential-model calculation [66]. For the strong coupling constant, we use the two-loop formula

$$\alpha_s(\mu_R) = \frac{4\pi}{\beta_0 \ln(\mu_R^2/\Lambda_{\text{QCD}}^2)} \left[ 1 - \frac{\beta_1 \ln \ln(\mu_R^2/\Lambda_{\text{QCD}}^2)}{\beta_0^2 \ln(\mu_R^2/\Lambda_{\text{QCD}}^2)} \right],$$

where  $\beta_1 = 34C_A^2/3 - 4T_F C_F n_f - 20T_F C_A n_f/3$  is the two-loop coefficient of the QCD  $\beta$ -function. According to  $\alpha_s(m_Z) = 0.1185$  [67], we obtain  $\Lambda_{\text{QCD}}^{n_f=5} = 0.233 \text{ GeV}$  and  $\Lambda_{\text{QCD}}^{n_f=4} = 0.337 \text{ GeV}$ .

### A. Basic results

The decay widths for  $W^+ \rightarrow B_c + b + \bar{s} + X$  and  $W^+ \rightarrow B_c^* + b + \bar{s} + X$  under the fixed-order approach are given in Tables I and II, where  $\Gamma_{\text{NLO}} = \Gamma_{\text{LO}} + \Gamma_{\text{NLO}}^{\text{Cor}}$  and  $\Gamma_{\text{NLO}}^{\text{Cor}}$  denotes the NLO corrections,  $\Gamma_{\text{NLO}}^{\text{Cor}} = \Gamma_{\text{virtual}}^{\text{Cor}} + \Gamma_{\text{Real}}^{\text{Cor}}$ . In the calculation, we take two typical energy scales ( $2m_b$  and  $m_W$ ) as the renormalization scale, and we have  $\alpha_s(2m_b) = 0.180$  and  $\alpha_s(m_W) = 0.121$ . Tables I and II show that the NLO corrections are significant. After including the NLO corrections, the total decay width for  $W^+ \rightarrow B_c(B_c^*) + b + \bar{s} + X$  is increased by 69% (43%) for  $\mu_R = 2m_b$  and 109% (92%) for  $\mu_R = m_W$ .

TABLE I. The total decay widths of  $W^+ \rightarrow B_c + b + \bar{s} + X$  up to NLO level under the fixed-order approach. Two typical renormalization scales are adopted.

	$\Gamma_{\text{LO}}$ (keV)	$\Gamma_{\text{NLO}}^{\text{Cor}}$ (keV)	$\Gamma_{\text{NLO}}$ (keV)	$\Gamma_{\text{NLO}}^{\text{Cor}}/\Gamma_{\text{LO}}$
$\mu_R = 2m_b$	2.89	2.00	4.89	0.69
$\mu_R = m_W$	1.30	1.42	2.72	1.09

TABLE II. The total decay widths of  $W^+ \rightarrow B_c^* + b + \bar{s} + X$  up to NLO level under the fixed-order approach. Two typical renormalization scales are adopted.

	$\Gamma_{\text{LO}}$ (keV)	$\Gamma_{\text{NLO}}^{\text{Cor}}$ (keV)	$\Gamma_{\text{NLO}}$ (keV)	$\Gamma_{\text{NLO}}^{\text{Cor}}/\Gamma_{\text{LO}}$
$\mu_R = 2m_b$	2.48	1.07	3.55	0.43
$\mu_R = m_W$	1.12	1.03	2.15	0.92

The momentum of the produced  $b$ -quark jet can be measured using vertex tagging technology, so the invariant mass of the  $B_c^{(*)}$  and  $b$  quark in the final state can be determined experimentally. We present the differential decay widths  $d\Gamma/ds_1$  for  $W^+ \rightarrow B_c(B_c^*) + b + \bar{s} + X$  in Figs. 4 and 5, where  $\mu_R = 2m_b$  and  $\mu_R = m_W$ , respectively. Here  $s_1 \equiv (p_1 + p_2)^2$ . Figures 4 and 5 show that there is a peak near the minimum value of  $s_1$ , indicating the dominant contributions of the decay processes come from the phase-space region near the threshold of producing the  $B_c(B_c^*)$  and  $b$  quark. This property may be helpful to distinguish the  $B_c$  or  $B_c^*$  mesons produced through the  $W^+$ -boson decays from the those produced through other production mechanisms at the high-energy colliders.

Tables I and II show that after including the NLO corrections, the renormalization scale dependence is softened. However, such scale dependence is still very large, e.g.,  $W^+ \rightarrow B_c(B_c^*) + b + \bar{s} + X$ , the NLO total decay

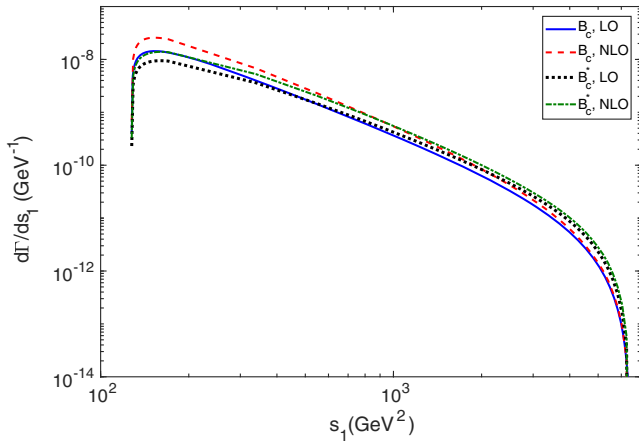


FIG. 4. Differential decay widths  $d\Gamma/ds_1$  for  $W^+ \rightarrow B_c(B_c^*) + b + \bar{s} + X$  under the fixed-order approach.  $\mu_R = 2m_b$ .

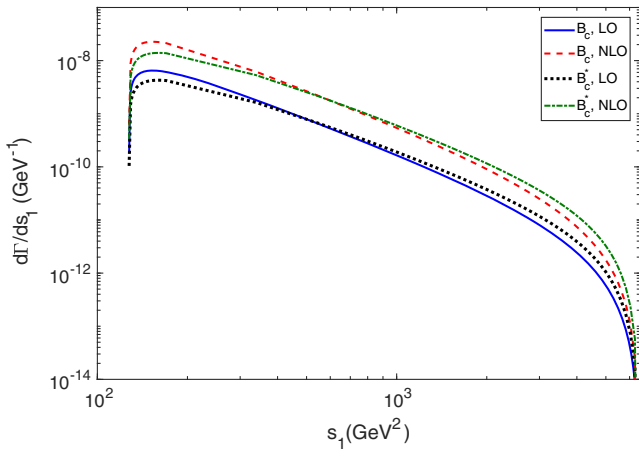


FIG. 5. Differential decay widths  $d\Gamma/ds_1$  for  $W^+ \rightarrow B_c(B_c^*) + b + \bar{s} + X$  under the fixed-order approach.  $\mu_R = m_W$ .

width decreases by 44% (39%), when  $\mu_R$  changes from  $2m_b$  to  $m_W$ .

As mentioned in the Introduction, the PMC scale-setting approach provides a way to eliminate the renormalization scale ambiguity [44–48]. As an attempt of showing how the PMC affects the decay width, we present the PMC predictions in the following.

To apply the PMC, we first schematically rewrite the NLO decay width as

$$\begin{aligned} \Gamma &= A\alpha_s^2(\mu_R) \left[ 1 + (a + bn_f) \frac{\alpha_s(\mu_R)}{\pi} \right] \\ &= A\alpha_s^2(\mu_R) \left\{ 1 + \left[ -\frac{3b}{2}\beta_0 + \left( a + \frac{33b}{2} \right) \right] \frac{\alpha_s(\mu_R)}{\pi} \right\}. \end{aligned} \quad (23)$$

Using the RGE, the nonconformal term  $(-\frac{3b}{2}\beta_0)$  can be adopted to fix the strong running coupling. A PMC scale  $\mu^{\text{PMC}}$  is then determined, which corresponds to the (correct) typical momentum flow of the process. Then, following the standard PMC procedures, the NLO decay width changes to

$$\Gamma_{\text{NLO}}^{\text{PMC}} = A\alpha_s(\mu^{\text{PMC}})^2 \left[ 1 + \left( a + \frac{33b}{2} \right) \alpha_s(\mu^{\text{PMC}}) \right], \quad (24)$$

where  $\mu^{\text{PMC}} = \mu_R e^{3b/2}$ . It is interesting to find that the PMC scale  $\mu^{\text{PMC}}$  is independent to any choice of renormalization scale  $\mu_R$ , e.g.,  $\mu^{\text{PMC}} \equiv 6.67$  GeV for  $B_c$  and  $\mu^{\text{PMC}} \equiv 7.17$  GeV for  $B_c^*$ , thus the conventional renormalization scale ambiguity is really eliminated. The PMC scales are closer to  $\mu_R = 2m_b$  than  $\mu_R = m_W$ , the conditions for the total decay widths are similar, thus the usual guessing choice of  $\mu_R = 2m_b$  is more reasonable for conventional prediction. Thus in the following analysis, we fix  $\mu_R = 2m_b$  for predictions when use conventional pQCD series.

Numerical results for the total decay widths of  $W^+ \rightarrow B_c(B_c^*) + b + \bar{s} + X$  up to NLO accuracy under the PMC are shown in Table III. After applying the PMC scale-setting approach, the convergence is slightly better than conventional series, e.g., after including the NLO QCD corrections, the decay width for  $W^+ \rightarrow B_c(B_c^*) + b + \bar{s} + X$  is increased by 58% (32%).

TABLE III. Total decay widths of  $W^+ \rightarrow B_c(B_c^*) + b + \bar{s} + X$  up to NLO accuracy under the PMC scale-setting approach.

	$\Gamma_{\text{LO}}$ (keV)	$\Gamma_{\text{NLO,Cor.}}$ (keV)	$\Gamma_{\text{NLO}}$ (keV)	$\Gamma_{\text{NLO,Cor.}}/\Gamma_{\text{LO}}$
$B_c$	3.53	2.05	5.58	0.58
$B_c^*$	2.92	0.92	3.84	0.32

### B. Comparison of the decay widths under the fixed-order and fragmentation approaches

It is interesting to know the differential distributions of those decay processes. We define the energy fraction  $z \equiv E_1/E_1^{\max}$ , where  $E_1$  and  $E_1^{\max}$  are the energy and the maximum energy of the  $B_c(B_c^*)$  meson in the rest frame of the initial  $W^+$ -boson. The differential decay widths  $d\Gamma/dz$  for  $W^+ \rightarrow B_c^* + b + \bar{s} + X$  are presented in Figs. 6 and 7. In addition to the fixed-order results, we also present the results from the fragmentation approach up to NLO level. Here, in order to know whether the fragmentation mechanism dominates the decay processes, we do not resum the leading logarithms of  $m_Q^2/m_W^2$ , i.e., the coefficient function and the fragmentation functions are both calculated at the

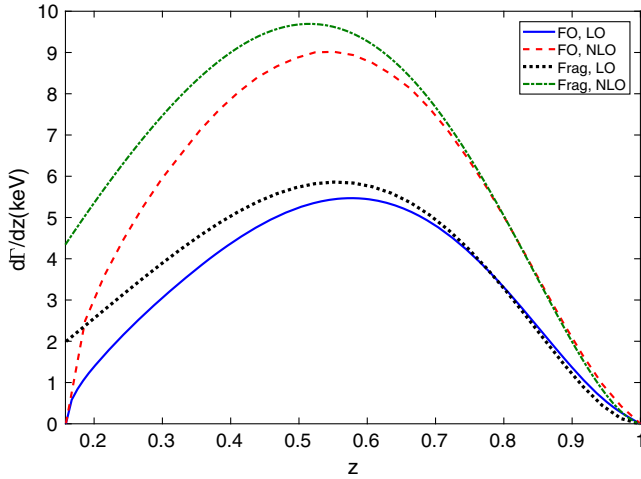


FIG. 6. The differential width  $d\Gamma/dz$  for  $W^+ \rightarrow B_c + b + \bar{s} + X$  under the fixed-order (FO) and fragmentation (Frag) approaches.

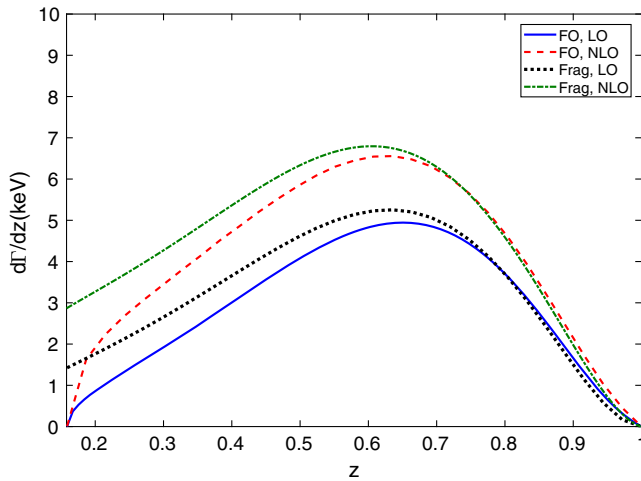


FIG. 7. The differential width  $d\Gamma/dz$  for  $W^+ \rightarrow B_c^* + b + \bar{s} + X$  under the fixed-order (FO) and fragmentation (Frag) approaches.

LO or NLO level without the DGLAP evolution. The factorization and renormalization scales are set as  $2m_b + m_c$  and  $2m_b$  respectively in the fragmentation calculation, and the renormalization scale is set as  $2m_b$  in the fixed-order calculation.

Figures 6 and 7 show that the fragmentation mechanism dominates the decay processes  $W^+ \rightarrow B_c(B_c^*) + b + \bar{s} + X$ , since the fixed-order and fragmentation shapes are close at the LO and NLO levels. Differences appear in the small  $z$  region, indicating in this  $z$  region, the nonfragmentation terms become important. The neglected logarithms of  $m_Q^2/m_W^2$  may give sizable contributions, which can be resummed in the fragmentation approach by using the DGLAP evolution equation. More explicitly, the NLO fragmentation results without or with resummation labeled as Frag, NLO and Frag, NLO + NLL are presented in Figs. 8 and 9, which are calculated by using Eqs. (20) and (21), respectively. The choices of the factorization and renormalization scales for the Frag, NLO and Frag, NLO + NLL calculations have been given below Eqs. (20) and (21) accordingly. Here the NLO fixed-order results labeled as “FO, NLO” are presented as a comparison. The decay widths for Frag, NLO and Frag, NLO + NLL are presented in Table IV. One may observe that by resumming the next-to-leading logarithms of  $m_Q^2/m_W^2$ , more accurate behavior in the large  $z$  region can be achieved, and the total decay widths shall be reduced by about 2% for both  $B_c$  and  $B_c^*$  productions.

In the fixed-order prediction, the large logarithms of  $m_Q^2/m_W^2$  may appear in the specific kinematic region, and the fragmentation approach provides us a way to give a reasonable contribution in this region by resumming all the large logarithms. Thus a combination of those two approaches may be helpful. As an attempt, we combine

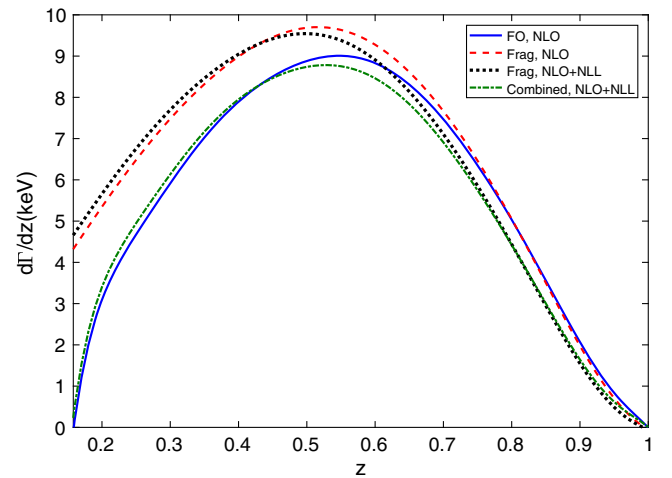


FIG. 8. The NLO differential decay width  $d\Gamma/dz$  for  $W^+ \rightarrow B_c + b + \bar{s} + X$  under the fixed-order approach (FO), fragmentation approach (Frag) and the combination of two approaches (Combined), respectively.

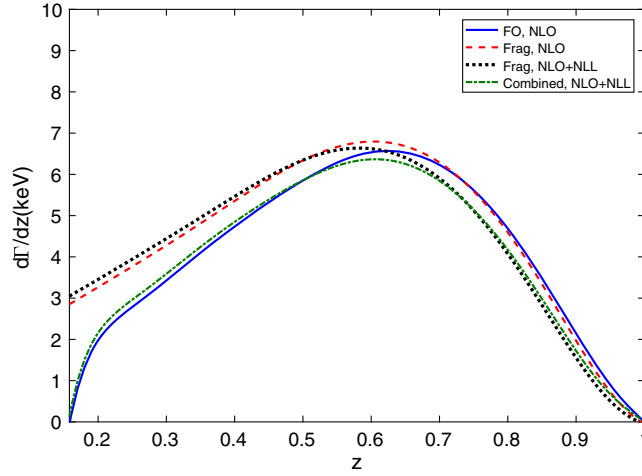


FIG. 9. The NLO differential decay width  $d\Gamma/dz$  for  $W^+ \rightarrow B_c^* + b + \bar{s} + X$  under the fixed-order approach (FO), fragmentation approach (Frag) and the combination of two approaches (Combined), respectively.

the NLO results from the fixed-order and fragmentation approaches in the following way:

$$d\Gamma_{W^+ \rightarrow B_c^{(*)} + X}^{\text{Combined, NLO+NLL}} = d\Gamma_{W^+ \rightarrow B_c^{(*)} + X}^{\text{FO, NLO}} + \left( d\Gamma_{W^+ \rightarrow B_c^{(*)} + X}^{\text{Frag, NLO+NLL}} - d\Gamma_{W^+ \rightarrow B_c^{(*)} + X}^{\text{Frag, NLO}} \right).$$

Here, the choices of the factorization and renormalization scales for the Frag, NLO and Frag, NLO + NLL calculations have been given below Eqs. (20) and (21) accordingly, and the renormalization for the ‘‘FO’’ calculation is set as  $\mu_R = 2m_b$ . The differential decay widths  $d\Gamma/dz$  for ‘‘Combined, NLO + NLL’’ are also presented in Figs. 8 and 9. The total decay widths are

$$\Gamma_{W^+ \rightarrow B_c + X}^{\text{Combined, NLO+NLL}} = 4.78 \text{ keV}, \quad (25)$$

$$\Gamma_{W^+ \rightarrow B_c^* + X}^{\text{Combined, NLO+NLL}} = 3.47 \text{ keV}. \quad (26)$$

These combined results are the definitive results in the presented paper because the large logarithms of  $m_Q^2/m_W^2$  have been resummed and the theoretical uncertainties are reduced compared to the fixed-order results.

TABLE IV. The total decay widths (in unit: keV) for  $W^+ \rightarrow B_c(B_c^*) + b + \bar{s} + X$  under the fragmentation approach.

	Frag, NLO	Frag, NLO + NLL
$B_c$	5.82	5.71
$B_c^*$	4.15	4.07

### C. Uncertainty analysis

In this subsection, we shall estimate the theoretical uncertainties for these decay widths. The main uncertainty sources for these decay widths include the heavy quark masses ( $m_c$  and  $m_b$ ), the renormalization scale and the radial wave function at the origin  $|R_S(0)|$ .  $|R_S(0)|^2$  is an overall factor in the calculation, the uncertainty due to it can be figured out easily. So we shall not consider the uncertainty of  $|R_S(0)|^2$  and concentrate our attention on the uncertainties from the heavy quark masses and the renormalization scale. To clarify, when considering the uncertainty caused by one input parameter, the other input parameters are fixed to their center values.

We first consider the uncertainties caused by the heavy quark masses. We estimate the uncertainties by varying the heavy quark masses with  $m_c = 1.5 \pm 0.1$  GeV and  $m_b = 4.9 \pm 0.2$  GeV. The uncertainties caused by  $m_c$  and  $m_b$  are presented in Tables V and VI respectively. For comparison, the fixed-order results and the combined NLO + NLL results are presented explicitly. From the two tables, we can see that the decay widths decrease with the increment of  $m_c$  and  $m_b$ , but they are more sensitive to  $m_b$  than  $m_c$ . Adding these two uncertainties caused by  $m_c$  and  $m_b$  in quadrature, we obtain the uncertainties caused by the heavy quark masses:

$$\begin{aligned} \Gamma_{W^+ \rightarrow B_c + X}^{\text{FO, NLO}} &= 4.89_{-0.65}^{+0.82} \text{ keV}, \\ \Gamma_{W^+ \rightarrow B_c^* + X}^{\text{FO, NLO}} &= 3.55_{-0.46}^{+0.59} \text{ keV}, \end{aligned} \quad (27)$$

and

$$\begin{aligned} \Gamma_{W^+ \rightarrow B_c + X}^{\text{Combined, NLO+NLL}} &= 4.78_{-0.63}^{+0.80} \text{ keV}, \\ \Gamma_{W^+ \rightarrow B_c^* + X}^{\text{Combined, NLO+NLL}} &= 3.47_{-0.45}^{+0.58} \text{ keV}. \end{aligned} \quad (28)$$

TABLE V. The decay widths (in unit: keV) for  $W^+ \rightarrow B_c(B_c^*) + b + \bar{s} + X$  with a variation of  $m_c = 1.5 \pm 0.1$  GeV.

$m_c$ (GeV)	1.4	1.5	1.6
$B_c$ (FO, NLO)	4.95	4.89	4.84
$B_c$ (Comb, NLO + NLL)	4.84	4.78	4.74
$B_c^*$ (FO, NLO)	3.57	3.55	3.53
$B_c^*$ (Comb, NLO + NLL)	3.50	3.47	3.46

TABLE VI. The decay widths (in unit: keV) for  $W^+ \rightarrow B_c(B_c^*) + b + \bar{s} + X$  with a variation of  $m_b = 4.9 \pm 0.2$  GeV.

$m_b$ (GeV)	4.7	4.9	5.1
$B_c$ (FO, NLO)	5.71	4.89	4.24
$B_c$ (Comb, NLO + NLL)	5.58	4.78	4.15
$B_c^*$ (FO, NLO)	4.14	3.55	3.09
$B_c^*$ (Comb, NLO + NLL)	4.05	3.47	3.02

Then we consider the uncertainties caused by the renormalization scale and the factorization scale. For the fixed-order results under the conventional scale setting, the uncertainties caused by the renormalization scale can be estimated by varying the renormalization scale between the two typical energy scales  $2m_b$  and  $m_W$ . The fixed-order results with  $\mu_R = 2m_b$  and  $\mu_R = m_W$  have been presented in Tables I and II, i.e.,  $\Gamma_{W^+ \rightarrow B_c + X}^{\text{FO,NLO}} \in [2.72, 4.89]$  keV and  $\Gamma_{W^+ \rightarrow B_c^* + X}^{\text{FO,NLO}} \in [2.15, 3.55]$  keV with a variation of  $\mu_R \in [2m_b, m_W]$ . These uncertainties caused by the choice of the renormalization scale in the fixed-order results are big.

For the combined NLO + NLL results, there are several renormalization and factorization scales involved in the calculation. We can decompose the combined NLO + NLL results into fragmentation contribution  $d\Gamma_{W^+ \rightarrow B_c^{(*)} + X}^{\text{Frag,NLO+NLL}}$  and power-correction contribution  $(d\Gamma_{W^+ \rightarrow B_c^{(*)} + X}^{\text{FO,NLO}} - d\Gamma_{W^+ \rightarrow B_c^{(*)} + X}^{\text{Frag,NLO}})$ . For the fragmentation contribution, there are lower factorization and renormalization scales, and upper factorization and renormalization scales involved in the calculation. The lower scales should be  $\mathcal{O}(m_Q)$  and the upper scales should be  $\mathcal{O}(m_W)$ . Since we adopt the approximation used in Ref. [65] where  $\int_0^1 dz P_{c \rightarrow c}(z) = 0$ , the fragmentation probabilities for  $c \rightarrow B_c(B_c^*)$  do not change under the DGLAP evolution. Thus, for the total decay widths, we need not consider the uncertainties caused by the lower and upper factorization scales, and only need to consider the uncertainties caused by the lower and upper renormalization scales. For the power-correction contribution, the renormalization scales in  $d\Gamma_{W^+ \rightarrow B_c^{(*)} + X}^{\text{FO,NLO}}$  and  $d\Gamma_{W^+ \rightarrow B_c^{(*)} + X}^{\text{Frag,NLO}}$  should be the same. We take the renormalization scales in the power-correction contribution as the same as the lower renormalization scale in the fragmentation contribution for simplicity. In order to estimate the uncertainties for the combined NLO + NLL results, we vary the lower and upper renormalization scales by a factor of 2 from their center values.

The decay widths with lower renormalization scale  $\mu_{R0} = 2m_b$  and  $\mu_{R0} = 4m_b$  are presented in Table VII, and the decay widths with upper renormalization scale  $\mu_R = m_W$  and  $\mu_R = m_W/2$  are presented in Table VIII. More explicitly, we obtain  $\Gamma_{W^+ \rightarrow B_c + X}^{\text{Combined,NLO+NLL}} \in [3.93, 4.78]$  keV and  $\Gamma_{W^+ \rightarrow B_c^* + X}^{\text{Combined,NLO+NLL}} \in [2.97, 3.47]$  keV with a variation of the lower renormalization scale  $\mu_{R0} \in [2m_b, 4m_b]$ , and  $\Gamma_{W^+ \rightarrow B_c + X}^{\text{Combined,NLO+NLL}} \in [4.78, 4.81]$  keV and  $\Gamma_{W^+ \rightarrow B_c^* + X}^{\text{Combined,NLO+NLL}} \in [3.47, 3.49]$  keV

TABLE VII. The combined, NLO + NLL decay widths (in unit: keV) with a variation of the lower renormalization scale  $\mu_{R0}$ .

$\mu_{R0}$	$2m_b$	$4m_b$
$B_c$	4.78	3.93
$B_c^*$	3.47	2.97

TABLE VIII. The combined, NLO + NLL decay widths (in unit: keV) with a variation of the upper renormalization scale  $\mu_R$ .

$\mu_R$	$m_W$	$m_W/2$
$B_c$	4.78	4.81
$B_c^*$	3.47	3.49

with a variation of upper renormalization scale  $\mu_R \in [m_W/2, m_W]$ .

The results in Tables VII and VIII show that the combined NLO + NLL results are more sensitive to the lower renormalization scale than the upper renormalization scale. Comparing the results in Tables VII and VIII with those in Tables I and II, we can see that after resumming the large logarithms of  $m_Q^2/m_W^2$ , the uncertainties caused by the choice of the renormalization scale are reduced explicitly.

## VI. SUMMARY

In the present paper, we have calculated the  $W^+$ -boson decays,  $W^+ \rightarrow B_c(B_c^*) + b + \bar{s} + X$ , up to NLO QCD corrections under the NRQCD framework. Both the fixed-order and fragmentation approaches are adopted for the calculations. The theoretical uncertainties are analyzed through varying the heavy quark masses and the renormalization scale. Our results show the NLO corrections are significant. Under the conventional scale-setting approach, the decay widths for  $W^+ \rightarrow B_c(B_c^*) + b + \bar{s} + X$  shall be increased by 69% (43%) for the case of  $\mu_R = 2m_b$  after including the NLO corrections. The scale dependence can be suppressed after including the NLO corrections, even though it is still large. By using the PMC, we show that the renormalization scale ambiguity can be eliminated for those two decay processes; thus they provide another successful application of the PMC.

The differential distributions  $d\Gamma/dz$  for the  $W^+$ -boson decays  $W^+ \rightarrow B_c(B_c^*) + b + \bar{s} + X$  have been given under the fixed-order and the fragmentation approaches, respectively. Our results show that both decay processes are dominated by the fragmentation mechanism, and the differences exist in the small  $z$  region. By combining the fixed-order prediction with the fragmentation approach to resum the leading and next-to-leading logarithms of  $m_Q^2/m_W^2$ , a more accurate distribution to the fixed-order prediction can be achieved.

The total  $W$ -boson decay width is  $\Gamma_W = 2.09$  GeV [67]. Using the combined results (25) and (26) from the fixed-order and fragmentation approaches, we obtain the branching fractions for the considered channels, e.g.,

$$\Gamma_{W^+ \rightarrow B_c + b + \bar{s} + X} / \Gamma_W = 2.29 \times 10^{-6}, \quad (29)$$

$$\Gamma_{W^+ \rightarrow B_c^* + b + \bar{s} + X} / \Gamma_W = 1.66 \times 10^{-6}. \quad (30)$$

If the LHC runs with a luminosity of  $10^{34} \text{ cm}^{-2} \text{ s}^{-1}$  [37], the expected  $W^+$ -boson events are about  $3.07 \times 10^{10}$  events per operation year. Then, there are about  $7.03 \times 10^4$   $B_c$  mesons and  $5.10 \times 10^4$   $B_c^*$  mesons to be produced through the  $W^+$ -boson decays per operation year. Two 2S-level excited states  $B_c(2^1S_0)$  and  $B_c(2^3S_1)$  have recently been observed by CMS and LHCb collaborations [68,69]. Using  $|R_{2S}(0)|^2 = 0.983 \text{ GeV}^3$  [66], there are about  $4.21 \times 10^4$   $B_c(2^1S_0)$  and  $3.05 \times 10^4$   $B_c^*(2^3S_1)$  to be produced through the  $W^+$ -boson decays per operation year. Those excited states can also be important sources for the ground-state  $B_c$  meson. Thus by carefully measuring the  $W^+$ -boson decays, we may have a good chance to study the  $B_c$ -meson properties.

## ACKNOWLEDGMENTS

This work was supported in part by the Natural Science Foundation of China under Grants No. 11625520, No. 11847222, No. 11847301, No. 11675239, No. 11535002, No. 11745006, and No. 11821505, by the Fundamental Research Funds for the Central Universities under Grant No. 2019CDJDWL0005, by the China Postdoctoral Science Foundation under Grant No. 2019M663432, by the Chongqing Special Postdoctoral Science Foundation under Grant No. XmT2019055, and by the graduate research and innovation foundation of Chongqing, China, under Grant No. CYB19065.

- 
- [1] F. Abe *et al.* (CDF Collaboration), Observation of the  $B_c$  Meson in  $p\bar{p}$  Collisions at  $\sqrt{s} = 1.8 \text{ TeV}$ , *Phys. Rev. Lett.* **81**, 2432 (1998); Observation of  $B_c$  mesons in  $p\bar{p}$  collisions at  $\sqrt{s} = 1.8 \text{ TeV}$ , *Phys. Rev. D* **58**, 112004 (1998).
- [2] C.-H. Chang and Y.-Q. Chen, The hadronic production of the  $B_c$  meson at Tevatron, CERN LHC and SSC, *Phys. Rev. D* **48**, 4086 (1993).
- [3] C.-H. Chang, Y.-Q. Chen, G.-P. Han, and H.-T. Jiang, On hadronic production of the  $B_c$  meson, *Phys. Lett. B* **364**, 78 (1995).
- [4] K. Kolodziej, A. Leike, and R. Ruckl, Production of  $B_c$  mesons in hadronic collisions, *Phys. Lett. B* **355**, 337 (1995).
- [5] A. V. Berezhnoy, A. K. Likhoded, and M. V. Shevlyagin, Hadronic production of  $B_c$  mesons, *Phys. At. Nucl.* **58**, 672 (1995).
- [6] C.-H. Chang, Y.-Q. Chen, and R. J. Oakes, Comparative study of the hadronic production of  $B_c$  mesons, *Phys. Rev. D* **54**, 4344 (1996).
- [7] A. V. Berezhnoy, V. V. Kiselev, and A. K. Likhoded, Hadronic production of S and P wave states of anti-b c quarkonium, *Z. Phys. A* **356**, 79 (1996).
- [8] S. P. Baranov, Pair production of  $B_c^{(*)}$  mesons in pp and gamma gamma collisions, *Phys. Rev. D* **55**, 2756 (1997).
- [9] S. P. Baranov, Semiperturbative and nonperturbative production of hadrons with two heavy flavors, *Phys. Rev. D* **56**, 3046 (1997).
- [10] K. M. Cheung,  $B_c$  meson production at the Tevatron revisited, *Phys. Lett. B* **472**, 408 (2000).
- [11] C.-H. Chang and X.-G. Wu, Uncertainties in estimating hadronic production of the meson  $B_c$  and comparisons between TEVATRON and LHC, *Eur. Phys. J. C* **38**, 267 (2004).
- [12] C.-H. Chang, J.-X. Wang, and X.-G. Wu, Hadronic production of the P-wave excited  $B_c$ -states  $B_{c(J,L=1)}^*$ , *Phys. Rev. D* **70**, 114019 (2004).
- [13] C.-H. Chang, C.-F. Qiao, J.-X. Wang, and X.-G. Wu, The color-octet contributions to P-wave  $B_c$  meson hadroproduction, *Phys. Rev. D* **71**, 074012 (2005).
- [14] C.-H. Chang, C.-F. Qiao, J.-X. Wang, and X.-G. Wu, Hadronic production of  $B_c(B_c^*)$  meson induced by the heavy quarks inside the collision hadrons, *Phys. Rev. D* **72**, 114009 (2005).
- [15] C.-H. Chang, C. Driouichi, P. Eerola, and X.-G. Wu, BCVEGPY: An event generator for hadronic production of the  $B_c$  meson, *Comput. Phys. Commun.* **159**, 192 (2004).
- [16] C.-H. Chang, J.-X. Wang, and X.-G. Wu, BCVEGPY2.0: An upgrade version of the generator BCVEGPY with an addendum about hadroproduction of the P-wave  $B_c$  states, *Comput. Phys. Commun.* **174**, 241 (2006); An upgraded version of the generator BCVEGPY2.0 for hadronic production of  $B_c$  meson and its excited states, *Comput. Phys. Commun.* **175**, 624 (2006).
- [17] X.-Y. Wang and X.-G. Wu, A trick to improve the efficiency of generating unweighted events from BCVEGPY, *Comput. Phys. Commun.* **183**, 442 (2012).
- [18] A. V. Berezhnoy, I. N. Belov, A. K. Likhoded, and A. V. Luchinsky,  $B_c$  excitations at LHC experiments, *Mod. Phys. Lett. A* **34**, 1950331 (2019).
- [19] Z. Yang, X.-G. Wu, and X.-Y. Wang, BEEC: An event generator for simulating the  $B_c$  meson production at an  $e^+e^-$  collider, *Comput. Phys. Commun.* **184**, 2848 (2013).
- [20] X.-C. Zheng, C.-H. Chang, and Z. Pan, Production of doubly heavy-flavored hadrons at  $e^+e^-$  colliders, *Phys. Rev. D* **93**, 034019 (2016).
- [21] X.-C. Zheng, C.-H. Chang, T.-F. Feng, and Z. Pan, NLO QCD corrections to  $B_c(B_c^*)$  production around the Z pole at an  $e^+e^-$  collider, *Sci. China Phys. Mech. Astron.* **61**, 031012 (2018).
- [22] X.-C. Zheng, C.-H. Chang, and T.-F. Feng, A proposal on complementary determination of the electro-weak mixing angles  $\sin \theta_W$  at a super Z-factory, [arXiv:1810.09393](https://arxiv.org/abs/1810.09393).
- [23] X.-C. Zheng, C.-H. Chang, T.-F. Feng, and X.-G. Wu, QCD NLO fragmentation functions for c or  $\bar{b}$  quark to  $B_c$  or  $B_c^*$  meson and their application, *Phys. Rev. D* **100**, 034004 (2019).
- [24] A. V. Berezhnoy, A. K. Likhoded, A. I. Onishchenko, and S. V. Poslavsky, Next-to-leading order QCD corrections to

- paired  $B_c$  production in  $e^+e^-$  annihilation, *Nucl. Phys.* **B915**, 224 (2017).
- [25] H.-Y. Bi, R.-Y. Zhang, H.-Y. Han, Y. Jiang, and X. G. Wu, Photoproduction of the  $B_c^{(*)}$  meson at the LHeC, *Phys. Rev. D* **95**, 034019 (2017).
- [26] K. He, H.-Y. Bi, R.-Y. Zhang, X.-Z. Li, and W.-G. Ma,  $P$ -wave excited  $B_c^{*}$  meson photoproduction at the LHeC, *J. Phys. G* **45**, 055005 (2018).
- [27] C.-F. Qiao, C.-S. Li, and K.-T. Chao, Top quark decays into heavy quark mesons, *Phys. Rev. D* **54**, 5606 (1996).
- [28] C.-H. Chang, J.-X. Wang, and X.-G. Wu, Production of  $B_c$  or  $\bar{B}_c$  meson and its excited states via  $t$ -quark or  $\bar{t}$ -quark decays, *Phys. Rev. D* **77**, 014022 (2008).
- [29] P. Sun, L.-P. Sun, and C.-F. Qiao, Next-to-leading order corrections to top quark decays to heavy quarkonia, *Phys. Rev. D* **81**, 114035 (2010).
- [30] C.-H. Chang and Y.-Q. Chen, The production of  $B_c$  or  $\bar{B}_c$  associated with two heavy quark jets in  $Z^0$  boson decay, *Phys. Rev. D* **46**, 3845 (1992); Erratum, *Phys. Rev. D* **50**, 6013 (1994).
- [31] L.-C. Deng, X.-G. Wu, Z. Yang, Z.-Y. Fang, and Q.-L. Liao,  $Z^0$  boson decays to  $B_c^{(*)}$  meson and its uncertainties, *Eur. Phys. J. C* **70**, 113 (2010).
- [32] Z. Yang, X.-G. Wu, L.-C. Deng, J.-W. Zhang, and G. Chen, Production of the  $P$ -wave excited  $B_c$ -states through the  $Z^0$  boson decays, *Eur. Phys. J. C* **71**, 1563 (2011).
- [33] C.-F. Qiao, L.-P. Sun, and R.-L. Zhu, The NLO QCD corrections to  $B_c$  meson production in  $Z^0$  decays, *J. High Energy Phys.* **08** (2011) 131.
- [34] J. Jiang, L.-B. Chen, and C.-F. Qiao, QCD NLO corrections to inclusive  $B_c^*$  production in  $Z^0$  decays, *Phys. Rev. D* **91**, 034033 (2015).
- [35] J. Jiang and C.-F. Qiao,  $B_c$  production in Higgs boson decays, *Phys. Rev. D* **93**, 054031 (2016).
- [36] Q.-L. Liao and J. Jiang, Excited heavy quarkonium production in Higgs boson decays, *Phys. Rev. D* **100**, 053002 (2019).
- [37] C.-F. Qiao, L.-P. Sun, D.-S. Yang, and R.-L. Zhu,  $W$  boson inclusive decays to quarkonium and  $B_c^{(*)}$  meson at the LHC, *Eur. Phys. J. C* **71**, 1766 (2011).
- [38] Q.-L. Liao, X.-G. Wu, J. Jiang, Z. Yang, and Z.-Y. Fang, Heavy quarkonium production at the LHC through  $W$  boson decays, *Phys. Rev. D* **85**, 014032 (2012).
- [39] F. Feng, Y. Jia, and W.-L. Sang, Optimized predictions for  $W \rightarrow B_c + \gamma$  combining light-cone and NRQCD approaches, arXiv:1902.11288.
- [40] G. T. Bodwin, E. Braaten, and G. P. Lepage, Rigorous QCD analysis of inclusive annihilation and production of heavy quarkonium, *Phys. Rev. D* **51**, 1125 (1995); Erratum, *Phys. Rev. D* **55**, 5853 (1997).
- [41] X.-G. Wu, S. J. Brodsky, and M. Mojaza, The renormalization scale-setting problem in QCD, *Prog. Part. Nucl. Phys.* **72**, 44 (2013).
- [42] X.-G. Wu, Y. Ma, S.-Q. Wang, H.-B. Fu, H.-H. Ma, S. J. Brodsky, and M. Mojaza, Renormalization group invariance and optimal QCD renormalization scale-setting, *Rep. Prog. Phys.* **78**, 126201 (2015).
- [43] X.-G. Wu, J.-M. Shen, B.-L. Du, X.-D. Huang, S.-Q. Wang, and S. J. Brodsky, The QCD renormalization group equation and the elimination of fixed-order scheme-and-scale ambiguities using the principle of maximum conformality, *Prog. Part. Nucl. Phys.* **108**, 103706 (2019).
- [44] S. J. Brodsky and X.-G. Wu, Scale setting using the extended renormalization group and the principle of maximum conformality: The QCD coupling constant at four loops, *Phys. Rev. D* **85**, 034038 (2012).
- [45] S. J. Brodsky and X.-G. Wu, Eliminating the Renormalization Scale Ambiguity for Top-Pair Production Using the Principle of Maximum Conformality, *Phys. Rev. Lett.* **109**, 042002 (2012).
- [46] S. J. Brodsky and L. D. Giustino, Setting the renormalization scale in QCD: The principle of maximum conformality, *Phys. Rev. D* **86**, 085026 (2012).
- [47] M. Mojaza, S. J. Brodsky, and X.-G. Wu, Systematic All-Orders Method to Eliminate Renormalization-Scale and Scheme Ambiguities in Perturbative QCD, *Phys. Rev. Lett.* **110**, 192001 (2013).
- [48] S. J. Brodsky, M. Mojaza, and X.-G. Wu, Systematic scale-setting to all orders: The principle of maximum conformality and commensurate scale relations, *Phys. Rev. D* **89**, 014027 (2014).
- [49] M. Beneke and V. A. Smirnov, Asymptotic expansion of Feynman integrals near threshold, *Nucl. Phys.* **B522**, 321 (1998).
- [50] B. W. Harris and J. F. Owens, The two cutoff phase space slicing method, *Phys. Rev. D* **65**, 094032 (2002).
- [51] T. Hahn, Generating Feynman diagrams and amplitudes with FeynArts 3, *Comput. Phys. Commun.* **140**, 418 (2001).
- [52] R. Mertig, M. Bohm, and A. Denner, FeynCalc—Computer-algebraic calculation of Feynman amplitudes, *Comput. Phys. Commun.* **64**, 345 (1991).
- [53] V. Shtabovenko, R. Mertig, and F. Orellana, New developments in FeynCalc 9.0, *Comput. Phys. Commun.* **207**, 432 (2016).
- [54] F. Feng, Apart: A generalized Mathematica apart function, *Comput. Phys. Commun.* **183**, 2158 (2012).
- [55] A. V. Smirnov, Algorithm FIRE—Feynman Integral REDuction, *J. High Energy Phys.* **10** (2008) 107.
- [56] T. Hahn and M. Perez-Victoria, Automatized one loop calculations in four-dimensions and D-dimensions, *Comput. Phys. Commun.* **118**, 153 (1999).
- [57] G. P. Lepage, A new algorithm for adaptive multidimensional integration, *J. Comp. Phys.* **27**, 192 (1978).
- [58] X.-C. Zheng, C.-H. Chang, and X.-G. Wu, NLO fragmentation functions of heavy quarks into heavy quarkonia, *Phys. Rev. D* **100**, 014005 (2019).
- [59] Y. L. Dokshitzer, Calculation of the structure functions for deep inelastic scattering and  $e^+e^-$  annihilation by perturbation theory in quantum chromodynamics, *Zh. Eksp. Teor. Fiz.* **73**, 1216 (1977) [*Sov. Phys. JETP* **46**, 641 (1977)].
- [60] V. N. Gribov and L. N. Lipatov, Deep inelastic ep scattering in perturbation theory, *Yad. Fiz.* **15**, 781 (1972) [*Sov. J. Nucl. Phys.* **15**, 438 (1972)].
- [61] G. Altarelli and G. Parisi, Asymptotic freedom in parton language, *Nucl. Phys.* **B126**, 298 (1977).
- [62] G. Curci, W. Furmanski, and R. Petronzio, Evolution of parton densities beyond leading order: The nonsinglet case, *Nucl. Phys.* **B175**, 27 (1980).
- [63] W. Furmanski and R. Petronzio, Singlet parton densities beyond leading order, *Phys. Lett. B* **97**, 437 (1980).

- [64] E. G. Floratos, D. A. Ross, and C. T. Sachrajda, Higher order effects in asymptotically free gauge theories. 2. Flavor singlet wilson operators and coefficient functions, *Nucl. Phys.* **B152**, 493 (1979); A. Gonzalez-Arroyo and C. Lopez, Second order contributions to the structure functions in deep inelastic scattering. 3. The singlet case, *Nucl. Phys.* **B166**, 429 (1980); E. G. Floratos, C. Kounnas, and R. Lacaze, Higher order QCD effects in inclusive annihilation and deep inelastic scattering, *Nucl. Phys.* **B192**, 417 (1981).
- [65] B. Mele and P. Nason, The fragmentation function for heavy quarks in QCD, *Nucl. Phys.* **B361**, 626 (1991).
- [66] E. J. Eichten and C. Quigg, Mesons with beauty and charm: Spectroscopy, *Phys. Rev. D* **49**, 5845 (1994), and references therein.
- [67] C. Patrignani *et al.* (Particle Data Group), Review of particle physics, *Chin. Phys. C* **40**, 100001 (2016).
- [68] A. M. Sirunyan *et al.* (CMS Collaboration), Observation of Two Excited  $B_c^+$  States and Measurement of the  $B_c^+(2S)$  Mass in  $pp$  Collisions at  $\sqrt{s} = 13$  TeV, *Phys. Rev. Lett.* **122**, 132001 (2019).
- [69] R. Aaij *et al.* (LHCb Collaboration), Observation of an Excited  $B_c^+$  State, *Phys. Rev. Lett.* **122**, 232001 (2019).